Exploiting LBL-assembled Au nanoparticles to enhance Raman signals for point-of-care testing of osteoporosis with excreta sample

Jian F. Sun[1] · **Xuan Liu[2]** · **Zhi R. Guo[3]** · **Jian Dong[4]** · **Yawen Huang[5]** · **Jie Zhang[1]** · **Hui Jin[5]** · **Ning Gu[1]**

Abstract Due to the intrinsic lack of specific biomarkers, there is an increasing demand for degenerative diseases to develop a testing method independent upon the targeting biomolecules. In this paper, we proposed a novel idea for this issue which was to analyze the characteristic information of metabolites with Raman spectrum. First, we achieved the fabrication of stable, uniform and reproducible substrate to enhance the Raman signals, which is crucial to the following analysis of information. This idea was confirmed with the osteoporosis-modeled mice. Furthermore, the testing results with clinical samples also preliminarily exhibited the feasibility of this strategy. The substrate to enhance Raman signal was fabricated by the layer-by-layer assembly of Au nanoparticles. The osteoporosis modeling was made by bilateral ovariectomy. Ten female mice were randomly divided into two groups. The urine and dejecta samples of mice were collected every week. Clinic urine samples were collected from patients with osteoporosis while the controlled samples were from the young students in our university. The LBL-assembled substrate of Au nanoparticles was uniform, stable and reproducible to significantly enhance the Raman signals from tiny amount of samples. With a simple data processing technique, the Raman signal-based method can effectively reflect the development of osteoporosis by comparison with micro-CT characterization. Moreover, the Raman signal from samples of clinic patients also showed the obvious difference with that of the control. Raman spectrum may be a good tool to convey the pathological information of metabolites in molecular level. Our results manifested that the information-based testing is possibly feasible and promising. Our strategy utilizes the characteristic information rather than the biological recognition to test the diseases which are difficult to find specific biomarkers. This will be greatly beneficial to the prevention and diagnosis of degenerative diseases. Also, we believe the combination of big bio-data and characteristic recognition will change the current paradigm of medical diagnosis essentially.

J. F. Sun and X. Liu contributed equally to this manuscript.

✉ Jian F. Sun
   sunzaghi@seu.edu.cn

✉ Ning Gu
   guning@seu.edu.cn

1 Jiangsu Key Laboratory of Biomaterials and Devices, School of Biological Science and Medical Engineering, Southeast University, Nanjing, China

2 School of Medicine, Southeast University, Nanjing, China

3 Second Affiliated Hospital of Nanjing Medical University, Nanjing, China

4 State Key Laboratory of Bioelectronics, School of Biological Science and Medical Engineering, Southeast University, Nanjing, China

5 Zhongda Hospital, Nanjing, China

1 Introduction

Going with the social olden, degenerative diseases, such as Alzheimer's disease, osteoporosis and even cancer, are increasingly becoming dangerous to public health [1–3]. Because these diseases occur with consenescence process, few people will think of doing the medical inspection regularly. Also, current diagnostic techniques actually lack the ability to discover these diseases in early stage accurately.

Taken the osteoporosis as an instance, the feasible diagnosis relies on the Dual Energy X-ray Absorptiometry (DEXA) which is an expensive item of medical inspection and harmful to human body to a certain extent. Obviously, nobody can do this inspection very frequently. More importantly, this technique can only indicate osteoporosis after bone tissue turns significantly porous. The reason why osteoporosis fails to be detected by serological examination is lack of the specific biomarkers [4]. Actually, all current techniques of early diagnosis are dependent upon the specific biomarkers of high sensitivity [5]. Unfortunately, this remains a challenge for the degenerative diseases.

An alternative to the specific biomarkers in diagnosis is the high-throughput information. This philosophy can date back to the traditional medicine of China. Doctors in ancient China made diagnosis mainly by discerning the traits of information one patient showed rather than the biomarkers. The information can come from pulse, complexion, odor and metabolite. Obviously, this method highly relies on the personal experiences and skills of doctor but the resolution capability of human is so limited that lots of tiny characteristics fail to be perceived. Furthermore, the characteristics just reflect the phenotypic variety of patients but are indirectly correlative with the disease-associated variety in molecular level. However, with development of big-data techniques, computer can be trained to extract new knowledge from the big data. Thus, if a huge mass of data can be available and processed properly through the highly sensitive measurement, the diagnosis based on the characteristic information may be feasible in clinic.

With the development of nanotechnology, Raman spectrum exhibits an increasingly promising role in biological detection of high throughput. Raman signal has high sensitivity, often called "molecular fingerprint" due to its capability of specifically reflecting the information about molecular structures [6, 7]. Moreover, another highlighted advantage is that Raman signal can be greatly enhanced if the measured object is coupled with a metal-nanostructured substrate [8]. The enhancement factor is even possibly over 1,000,000. This surface enhanced Raman scattering (SERS) signal is very suitable to detect the trace amount of biological matters.

For the SERS-based biological detection, the substrate of nanostructure and the sample are of great importance. The substrate should be stable, homogenous and easily available while the sample should have activity of Raman signal and can be effectively enhanced by the substrate. Since that osteoporosis is a disease which features bone loss and abnormal endocrine [9], it is taken for granted that the excreta can reflect this disorder. Actually, ancient doctors have made diagnosis based on the color, odor and other characters of dejecta or urine for a long history. The excreta have some advantages over the blood or the serum.

For one thing, it is non-invasive. For another, it can exclude the influence of macromolecules such as protein. Because of the relatively large size and the complex structure, the accurate identification of characteristic signals for a huge amount of macromolecules remains challenging for SERS-based detection [10]. Besides, the macromolecules having the big size may cause the Raman-active groups far away from the substrate so that the detected signals are actually the Raman signals rather than the SERS signals. In this case, the signal will be too weak to recognize.

Here, we proposed a novel concept to employ SERS to detect osteoporosis directly with excreta sample. Mouse was used as animal model. This strategy is label-free and dependent upon the enhancement of substrate. The substrate which was fabricated by lay-by-layer (LBL) assembly of mono-dispersed gold nanoparticles exhibited good homogeneity and stability. The dejecta and urine of osteoporosis-modeled mice were measured, showing a visible difference in the Raman spectra with that of the control. This method was also applied for the clinic samples. The results proved the feasibility for human. This strategy is suitable for point-of-care testing because it is convenient, safe and capable of self-operation daily. Due to the independence upon biomarkers, the cost of this strategy is low which is important for extensive application in developing areas as well as in the poverty population.

Here, it should be mentioned that the SERS substrate will play an important role in the information-based diagnosis because it is the source of data. There have been many reports about the fabrication of SERS substrate. A common principle is to construct an array composed by Au or Ag nanoparticles with a certain distance to form the so-called hot spots. Certainly, the substrate should be homogeneous, uniform, stable and reproducible. The difficulty currently lies in the large scale. For the practical application, the sample is often randomly spotted or spread on the substrate. Therefore, the substrate should be good in the macroscopic scale rather than the scale of electronic microscopy. In our opinion, the order of nanoparticles for SERS substrate is unnecessary in single-particle level. Due to the restriction of machine, the detected signals actually come from the sum of signals enhanced by all the nanoparticles in one facula. The minimal diameter of one facula for the common Raman spectroscopy machines is about in several micrometers. Thus, it is adequate for the substrate to be ordered in level of several micrometers rather than nanometers. One simple method in practical application is to use sputtering. However, the size of single particle is very hard to control so that the final performance is also poor. The LBL method can integrate the mono-dispersed size of individual nanoparticles and the order in the micrometer scale so that it is considered this method will get an advantage over the sputtering method [11].

2 Experimental method

2.1 Synthesis of Au nanoparticles

20 nm colloidal Au was prepared through the classical citric acid reduction of $HAuCl_4$ in water with sodium citrate at near-boiling temperature. To effectively control the colloidal size, the three-necked flask was closed with a reflux condenser and the flask was heated spherically. After reaction, the nanoparticles were purified by centrifugal separation and free of further modification. Finally, the volume of colloidal Au was calibrated to 100 ml.

2.2 Layer-by-layer assembly

The above-mentioned colloidal Au was concentrated 10 times for the layer-by-layer assembly. Commercially available PDDA (poly-diallydimethylammonium chloride) was diluted to 1% with ultra-pure water. A glass slide was first treated by the boiling mixture of H_2SO_4 and H_2O_2 for 2h. After that the glass slide was washed by the ultra-pure water repeatedly and finally dried by N_2

gas stream. Then, the glass slide was put into the PDDA solution and the colloidal Au suspension for 15 and 25 min, respectively. The colloidal Au nanoparticles were adsorbed on the glass slide due to the electrostatic interaction which brought about the formation of one bilayer. When the soak in one solution terminated, the glass slide was washed by ultra-pure water repeatedly and finally dried by N_2 gas stream. The washing is important. Otherwise, the colloidal suspension will become instable. The steps were duplicated leading to the layer-by-layer assembly of nanoparticles.

2.3 Osteoporosis modeling of mouse

Ten female C57/BL6 mice of 8 months old were randomly divided into two groups. One was for establishing the osteoporosis model by bilateral ovariectomy (OVX). The other was treated with the sham surgery which was to perform the same operation as the ovariectomy but the excision was the body fat of equivalent weight rather than the ovarium. During the experimental period, both groups were fed with the same food-intake.
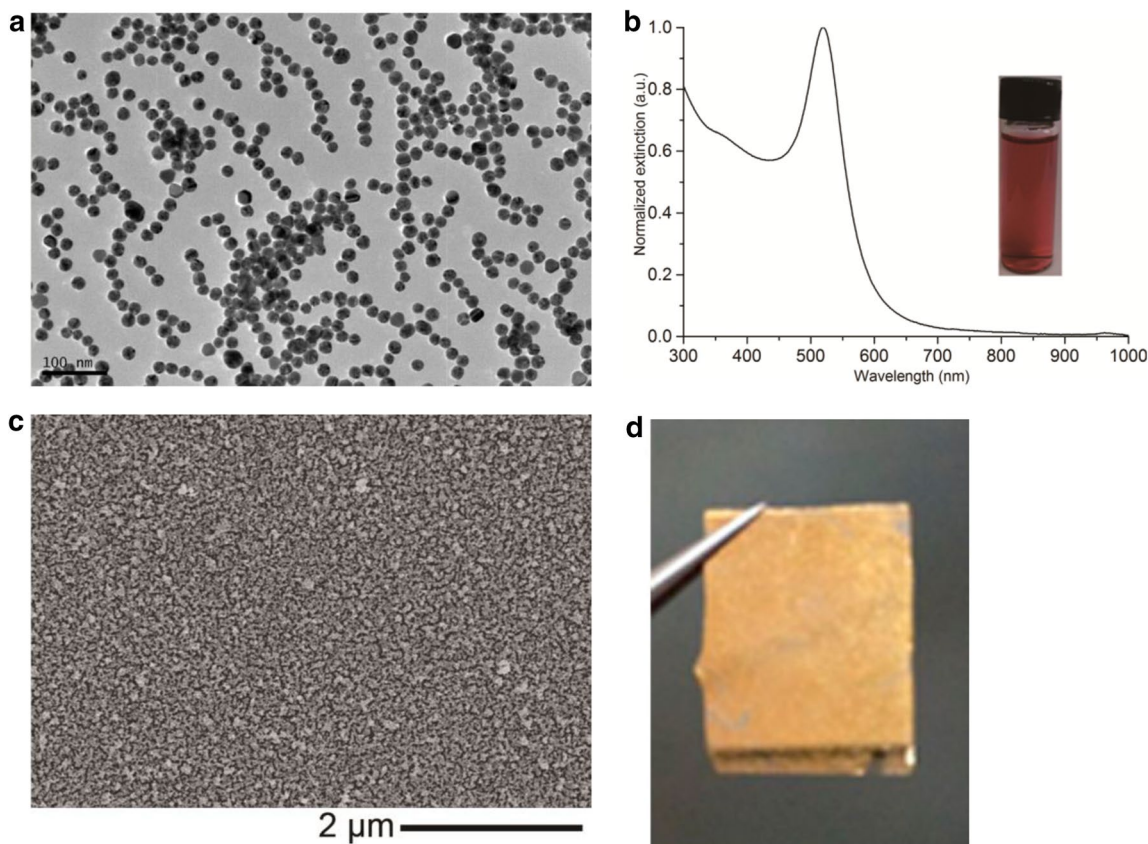
Fig. 1 Characterization of gold nanoparticles. **a** TEM image of synthesized colloidal Au. **b** UV spectrum measurement of synthesized colloidal Au. **c** SEM image of assembled Au nanoparticles after 7 bilayers. **d** Macroscopic photograph of assembled colloidal Au film
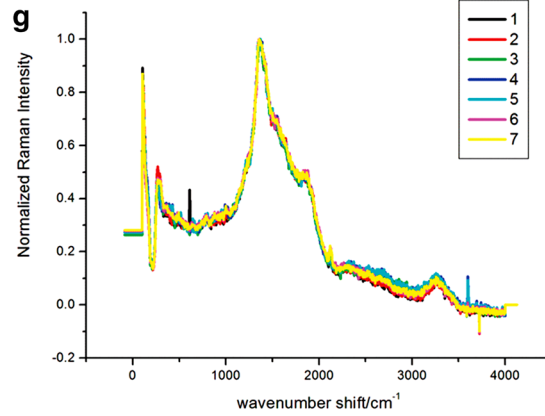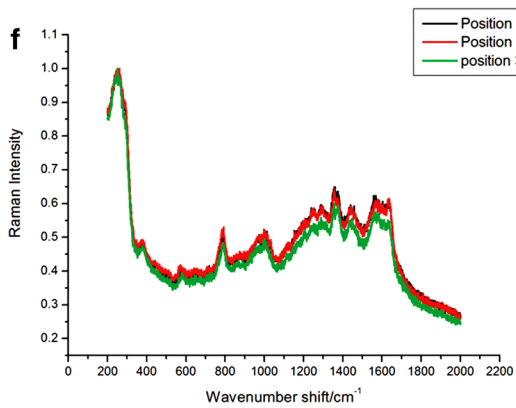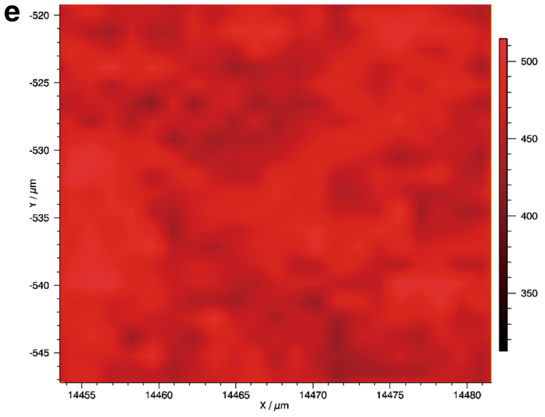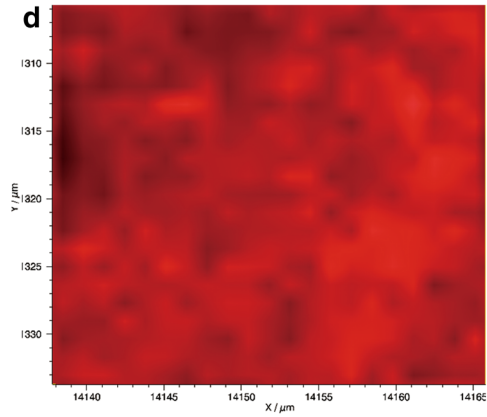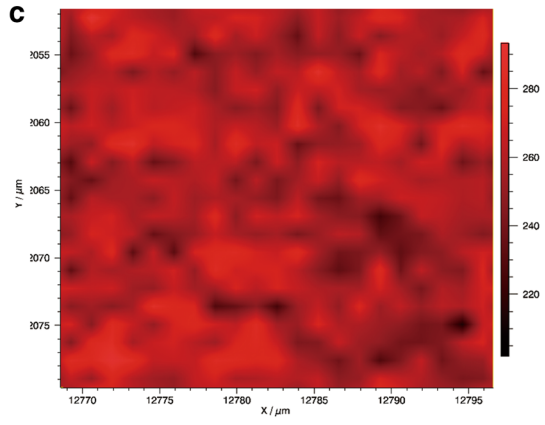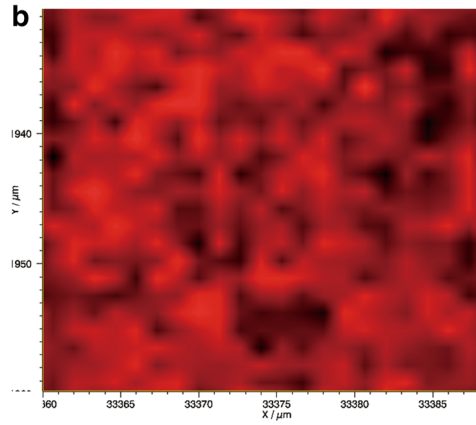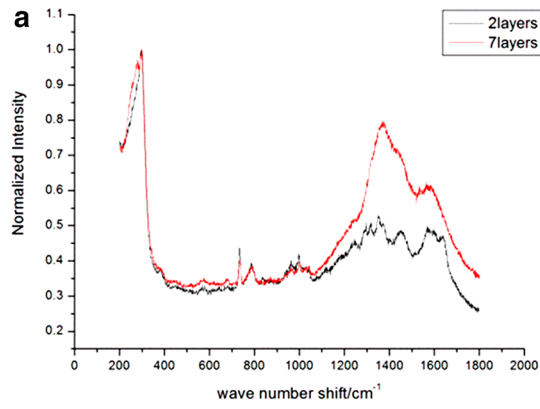
◀**Fig. 2** Raman spectroscopic evaluation of LBL-assembled film of colloidal Au. **a** Raman spectra of 2-layered film and 7-layered film. **b–e** Raman mapping of 3-layered film, 5-layered film, 7-layered film and 10-layered film, respectively. **f** Raman spectra of three arbitrary positions in one film after 7-layered assembly. **g** Raman spectra of one arbitrary position in seven films after 7-layered assembly

3 Results and discussion

The gold nanoparticles were synthesized by the classic method of chloroauric acid reduced by sodium citrate. The reaction parameters were optimized to control the colloidal size which was characterized by TEM (Electronic Microscopy) and UV (Ultraviolet) spectrum (Fig. 1a, b). Both results manifested that the synthesized colloidal Au possessed good monodispersity, which guaranteed the homogeneity of building blocks. This was fundamental and critical for the subsequent procedure of self-assembly.

The LBL assembly was based on the electrostatic interaction between the gold nanoparticles and the polyelectrolyte (PDDA, poly-diallydimethylammonium chloride) [12]. It is suitable for fabrication of SERS substrate because the homogeneity, uniformity and compatibility can be greatly improved with the increase of layer number. With the increase of assembled layers, the LBL film was observed to show a visible transition from red color to golden color with the naked eyes. This case indicated that the gold nanoparticles turned more and more compact. The SEM image of assembly morphology after 7 bilayers is shown in Fig. 1c and the photograph of the assembled film is shown in Fig. 1d. Seen from the images, the nanoparticles were aggregated together with disorder microscopically. However, the film was homogeneous, uniform and compact macroscopically. This trait was increasingly clear with the augment of assembled layers. From the local magnification, the surface of nanoparticles was capped by an organic layer which should be PDDA (Supporting Information, Fig. S1). Thus, the nanoparticles were non-contacting. The distance between two nanoparticles was the double thickness of the capping molecular layer. This was beneficial to the Raman enhancement because the space between nanoparticles was a natural hotspot which can further enhance the Raman signals.

With the number of assembled bilayer increasing, it was discovered by measurement of Raman spectroscopy that the uniformity and signal enhancement of nanoparticulate film was greatly improved. Figure 2a showed the Raman spectra of 2-bilayered LBL-assembled film and 7-bilayered film after data normalization. It was obvious that the Raman signals from 1400 to 1600 cm^{-1} were greatly enhanced. Here, the signals should be attributed to the PDDA molecules. This case can be furthermore confirmed by Raman mapping of different layered samples. The results were shown

in Fig. 2b–e, where the color turned increasingly uniform and the signal intensity also became higher. Interestingly, although the arrangement of Au nanoparticles should be disordered on substrate essentially resulting from the LBL assembly, the enhancement of Raman signal seemed uniform. However, we do not think the assembled layers are the more the better. When the assembled film was up to 40 layers, the enhancement just showed a little more than that of 10-layered film (Supporting Information, Fig. S2). Actually, if the assembled film is too compact and the nanoparticles are too much, there will be strong interactions between the gold nanoparticles. Then the film can be regarded as a macroscopically continuous medium more than a discrete nanoparticulate film in plasmonic property. In this case, the property of Raman signal enhancement will even be weakened. Therefore, a suitable density of nanoparticles was important for the fabrication of SERS substrate.

After assembly of seven layers, we arbitrarily chose three positions on one film for Raman detection. The results are shown in Fig. 2f, where it was seen that the curves were nearly coincident after data normalization. This case meant the film fabricated by the LBL assembly owned good uniformity. It was taken for granted that the uniformity will remain good with the assembled layers increasing. Furthermore, seven films were fabricated by different operators in different time. We arbitrarily chose one position in one film and measured the Raman spectra for the seven films after 7-layered assembly to evaluate the reproducibility. The result is shown in Fig. 2g, where the curves also matched fairly well. This case indicated that the nanoparticulate film fabricated by LBL assembly owned good reproducibility and was suitable to be employed as the SERS substrate.

The dejecta sample was marinated in the pure water and ultrasonically treated until the morphology of sample in suspension was invariable. Then the suspension was settled over night and the supernatant was extracted for measurement. The urine sample was directly put on the film as a droplet. The volume of sample was 2 μl and the measurement was operated after the solution was dried thoroughly. Here, the LBL-assembled film of colloidal Au was of great importance. If the sample was directly put on the silicon substrate for Raman detection, there will be just a peak of silica (Supporting Information, Fig. S3). This may result from the too small amount of detectable molecules in sample. However, in the presence of the LBL-assembled film of gold nanoparticles, it was seen that the spectra exhibited a visible difference between the control sample and the modeled sample (Supporting Information, Fig. S4). After the normalization, it was discovered that the difference was mainly in the range from 300 to 1200 cm^{-1}. The molecules in excreta can account for this difference. With the development of osteoporosis, the lost calcium from bone will form some complexes in vivo, finally passing out of
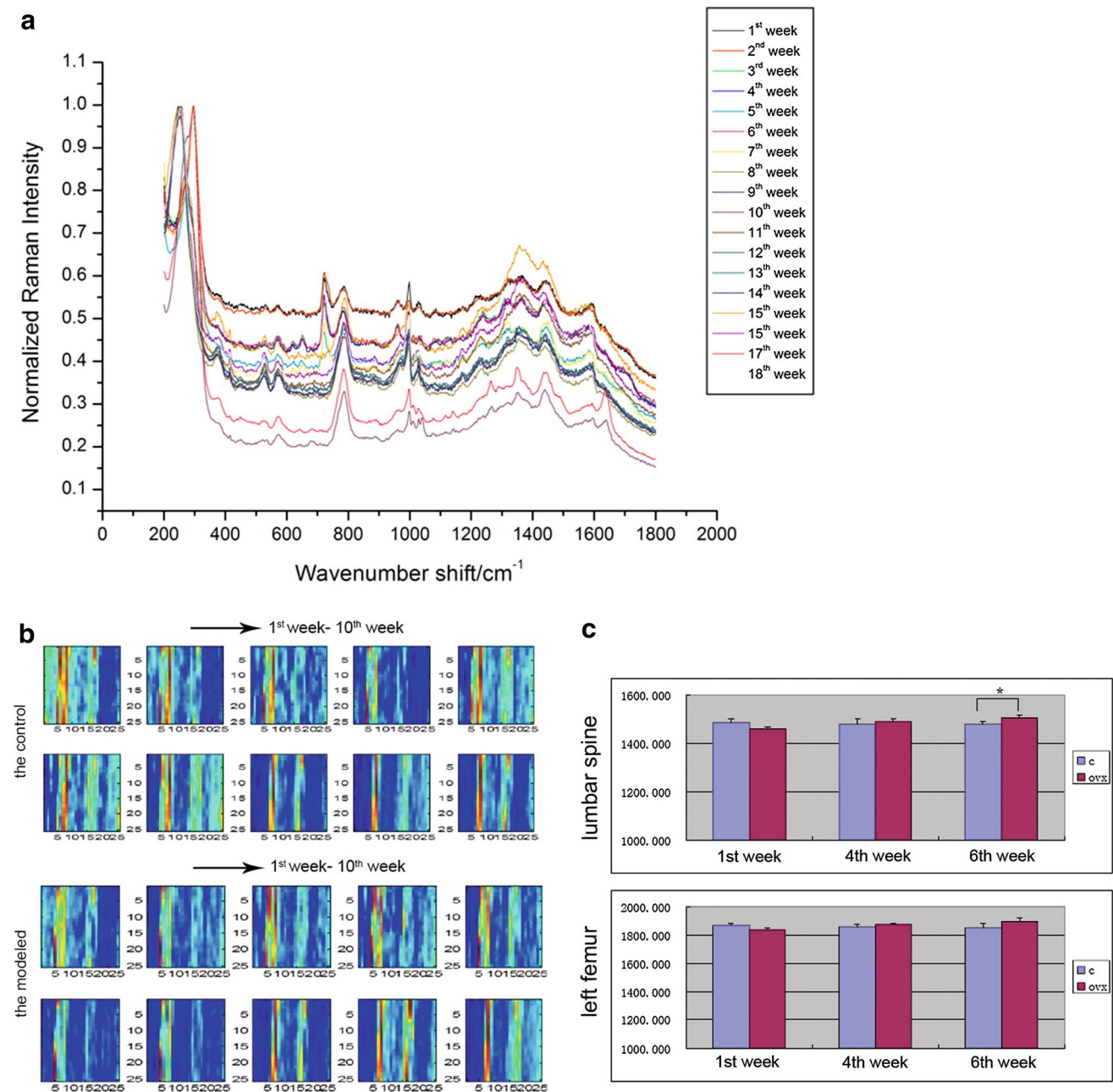
Fig. 3 Osteoporosis detection for the modeled mice. **a** Raman spectroscopic method. **b** Images after data transformation from the Raman spectroscopic curves into the two-dimensional images (pay attention to *red box*). **c** bone density evaluation of modeled mice with two body parts ($p < 0.05$). c means the control mice and ovx means the modeled mice

the body. These matters were reported to include C- and N-telopeptide of type I callagen [13, 14], deoxypyridinoline [15], cis-4-Hydroxy-L-proline [16] and so on, which have the Raman characteristic peaks in 500–600, 700, and 1000 cm^{-1}, respectively. Thus, it is true that the Raman signals can potentially reflect the variety of metabolite caused by osteoporosis. The data were also processed by Fast Fourier Transformation (FFT) and Power Spectrum Density (PSD), which are the common processing tools for the raw

data. Surprisingly, the processed data became totally identical. This case exhibited that the data processing method should be carefully chosen. In addition, the measurement with urine sample showed the similar result (Supporting Information, Fig. S5). However, for the mouse model, the collection of dejecta is much easier than that of urine so that the dejecta sample was chosen for detection with Raman spectrum in the following experiments. Actually, the dejecta sample underwent a leaching process before
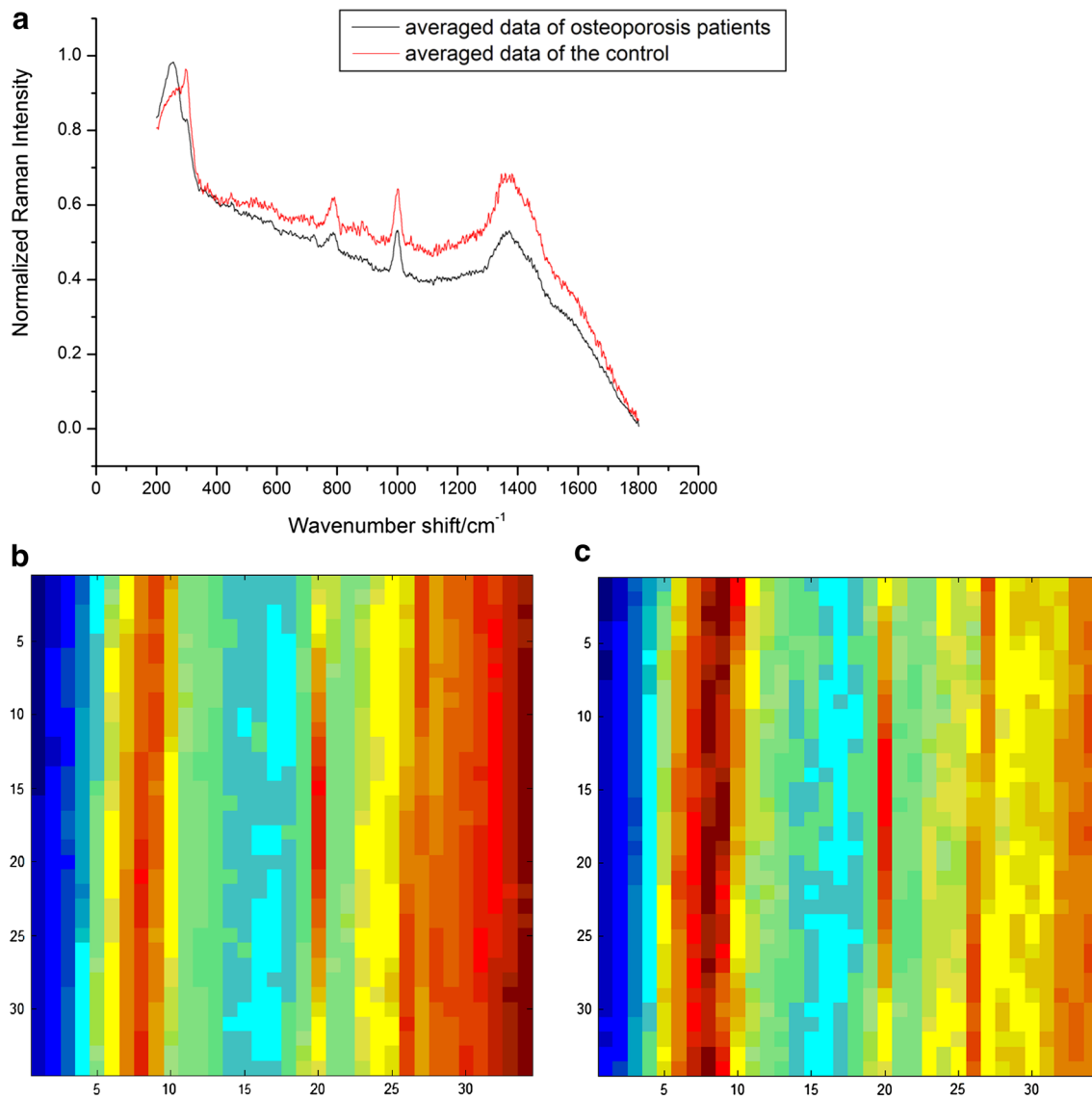
Fig. 4 Raman spectroscopic testing of clinic samples. **a** Raman spectroscopic curves of averaged data from osteoporosis patients and the control. **b–c** corresponding patterns transformed from **a**

the measurement and it was the extractive substance to be detected by Raman equipment. Thus, the detected sample was mainly the water-soluble molecules so that it was suitable for Raman detection.

In our experiments, ten mice were divided into two groups. One was the control and the other was the model of osteoporosis. The mice were fed under the unified and standard conditions. The sampling and the measurement were made every one week until the 18th week. After data collection, the average values of every week were calculated based on the 5 spectra. Thus, 18 curves of Raman spectroscopy were available (Fig. 3a) which also exhibited the difference in the range from 300 to 1200 cm^{-1}. However, the data were hard to recognize. Thus, signal processing is

needed to clarify the data. It was found that the visualization of difference can be greatly improved by transforming the one-dimensional signal into two-dimensional image. The results are shown in Fig. 3b (data of ten weeks were shown here and the images after 10th week were identical), seen from which the pattern began to exhibit alteration from the 4th week and the difference between the modeled sample and the control sample was maximized in the 6th week. After then, the patterns were becoming similar. This phenomenon matched the feature of modeling method which was realized by cutting the gonadal tissue to alter the endocrine. Because the metabolism can return into balance by the endocrine regulation, the difference between the control sample and the modeled sample will disappear after

a certain period. This case was also confirmed by the detection with micro-CT imaging. The results of bone density based on the micro-CT imaging are shown in Fig. 3c, seen from which the significant difference emerged in the 6th week. Here, the bone density value was also available by averaging the data from five mice. During the experiments of micro-CT imaging, two body parts were checked. One was the lumbar spine and the other was the left femur. The results on both body parts were same. The bone density value based on the X-ray imaging was the gold standard for the diagnosis of osteoporosis. However, due to the radiation and the cost, the X-ray is unsuitable to be used for point-of-care testing daily. This comparison confirmed the validity of our method. Here, it should be mentioned that this information-based diagnosis has better expandability than the biomarker-based diagnosis. For the same data, different data processing will bring about different information while the biomarker is uniquely specific.

Although the detailed relationship between SERS peaks and biological molecules still remained unclear, the Raman signal-based method seemed feasible for the testing of osteoporosis. Thus, we performed the testing of human samples to preliminarily verify the feasibility of this method in clinic. For human, the testing was done with urine sample. The urine samples were obtained from ten patients who were diagnosed with osteoporosis in Zhongda Hospital. The control samples were from six students in Southeast University who were below 23 years old. It has been extensively accepted that osteoporosis seldom happens to the youngster. The data of individual sample showed some variance but the averaged data of osteoporosis patients and the control still showed significant difference which can be recognized more facilely after transformation into two-dimensional pattern (Fig. 4). The results of human samples indicated the feasibility of this method in clinic. However, due to the complexity of human metabolite, signal processing should be more sophisticated. Recently, machine learning provides a promising tool for the information-based diagnosis. We believe this method can be accurate and applicable for many diseases after a huge mass of Raman data are available.

4 Conclusion

In conclusion, we proposed a novel method for point-of-care testing of osteoporosis. This method was based on the SERS detection of metabolite. Raman signal can reflect the information in the molecular level and was independent upon the biomarkers so that this method was especially suitable to the point-of-care testing of aging-relative diseases, such as the osteoporosis. To amplify the Raman signals, we developed a stable, homogeneous and large-scaled film of assembled colloidal Au as the measurement substrate with layer-by-layer assembly. Due to the good properties of substrate, it was discovered that the Raman data after normalization can well reflect the pathological difference between the osteoporosis samples and the control for both the modeled mice and the clinic patients, showing the feasibility of this strategy. We furthermore exploited a signal processing method to enhance the recognition of characteristics. Due to cheapness, safety and expandability, it is believed that our method will show its promising application in the POCT areas.

References

1. B. Strooper et al., Learning by failing: ideas and concepts to tackle γ-Secretases in Alzheimer's disease and beyond. Annu. Rev. Pharm. Toxic **55**, 419–437 (2015)
2. P. Andreopoulou et al., Management of postmenopausal osteoporosis. Annu. Rev. Med **66**, 329–342 (2015)
3. S. Hansen et al., A review of the equine age-related changes in the immune system: Comparisons between human and equine aging, with focus on lung-specific immune-aging. Ageing Res. Rev. **20**, 11–23 (2015)
4. T. Floerkemeier et al., Bone turnover markers failed to predict the occurrence of osteonecrosis of the femoral head—a preliminary study. J. Clin. Lab. Anal. **26**, 55–60 (2012)
5. R. Liu et al., Early diagnosis of complex diseases by molecular biomarkers, network biomarkers, and dynamical network biomarkers. Med. Res. Rev. **34**, 455–478 (2014)
6. A.C.S. Talari et al., Raman spectroscopy of biological tissues. Appl. Spectros. Rev. **50**, 46–111 (2015)
7. C.H. Camp et al., High-speed coherent Raman fingerprint imaging of biological tissues. Nat. Photon. **8**, 627–634 (2014)
8. LeE.C. Ru et al., Single-molecule surface-enhanced Raman spectroscopy. Annu. Rev. Phys. Chem. **63**, 65–87 (2012)
9. T.S. Orchard et al., A systematic review of omega-3 fatty acids and osteoporosis. British J. Nutrition **107**, S253–S260 (2012)
10. F. Pozzi et al., Sample treatment considerations in the analysis of organic colorants by surface-enhanced Raman scattering. Anal. Chem. **84**, 3751–3757 (2012)
11. Y. Li et al., "Layer-by-layer assembly for rapid fabrication of thick polymeric films". Chem. Soc. Rev **41**, 5998–6009 (2012)
12. Y. Kim et al., Stretchable nanoparticle conductors with self-organized conductive pathways. Nature **500**, 59–63 (2013)
13. M.A. García-Pérez et al., Similar efficacy of low and standard doses of transdermal estradiol in controlling bone turnover in postmenopausal women. Gynecol. Endocrinol. **22**, 179–184 (2006)
14. H. Hansdóttir et al., The effect of raloxifene on markers of bone turnover in older women living in long term care facilities. J. Am. Geriatr. Soc. **52**, 779–783 (2004)

15. S. Onodera et al., Transgenic mice overexpressing macrophage migration inhibitory factor (MIF) exhibit high-turnover osteoporosis. J. Bone Miner. Res. **21**, 876–885 (2006)

16. K.E. Effenberger et al., Regulation of osteoblastic phenotype and gene expression by hop-derived phytoestrogens. J. Steroid Biochem. Mol. Biol. **96**, 387–399 (2005)